Room and high temperature mechanical properties of Mg2Si, Mg2Sn and their solid solutions

Gustavo Castillo-Hernandez*

Institute of Materials Research, German Aerospace Center, 51170 Cologne, Germany and Institute of Inorganic and Analytical Chemistry, Justus Liebig University Giessen, Heinrich-Buff-Ring 17, 35392 Giessen, Germany, Gustavo.castillo-hernandez@dlr.de

Mohammad Yasseri

Institute of Materials Research, German Aerospace Center, 51170 Cologne, Germany and Institute of Inorganic and Analytical Chemistry, Justus Liebig University Giessen, Heinrich-Buff-Ring 17, 35392 Giessen, Germany, Mohammad.yasseri@dlr.de

Benedikt Klobes

University of Applied Sciences Bremerhaven, An der Karlstadt 8, 27568 Bremerhaven, Germany, bklobes@hs-bremerhaven.de

Sahar Ayachi

Institute of Materials Research, German Aerospace Center, 51170 Cologne, Germany, Sahar.ayachi@dlr.de

Eckhard Müller

Institute of Materials Research, German Aerospace Center, 51170 Cologne, Germany and Institute of Inorganic and Analytical Chemistry, Justus Liebig University Giessen, Heinrich-Buff-Ring 17, 35392 Giessen, Germany, Eckhard.mueller@dlr.de

Johannes de Boor‡

Institute of Materials Research, German Aerospace Center, 51170 Cologne, Germany, Johannes.deBoor@dlr.de

*corresponding author +4922036013357

‡ corresponding author +4922036014037

Abstract

Knowledge of the mechanical properties of thermoelectric materials at high temperature is required for the modelling and optimization of a thermoelectric

generator under application conditions. We present room and high temperature characterization of Young´s modulus for Mg_2Si, Mg_2Sn and their solid solutions establishing a linear dependence, both on composition and on temperature.

Through the comparison of Resonant Ultrasound Spectroscopy and free vibration techniques, we measure the elastic moduli with high precision. The comparison of our results (E = 110 GPa for Mg_2Si and 78 GPa for Mg_2Sn) to first principles calculations and experimentally reported data shows good agreement. Additionally, by estimating the Poisson ratio, we calculate the temperature-dependent shear modulus G and finally provide a simple bilinear function for Young´s and shear moduli as a function of temperature and composition.

Keywords: Thermoelectric, mechanical properties, magnesium silicide, magnesium stannide, Mg_2Si, Mg_2Sn

1. Introduction

Thermoelectric generators (TEG) for thermal-to-electric energy conversion in their most basic form consist of both n- and p-type doped semiconductor materials (commonly referred to as legs) electrically connected by a metallic bridge. Such devices have attracted the attention of researchers due to their inherent advantages such as simple construction, free scalability, lack of moving parts, and reduced maintenance cost and effort [1-3]. Their ability to perform under vacuum and in the absence of light also makes them perfect candidates for space mission energy supply, as exemplified by the Voyager missions and numerous further deep space and lander missions from the 1970´s [4]. TEGs can also be used in/are also candidates for terrestrial applications, such as waste heat recovery in industrial facilities, combustion engines and mobile or autarkic current supply e.g. for sensors.

Current TEG technology is mainly based on rare or toxic materials such as Te or Sb, which makes the “en masse” application of thermoelectric generators unattractive [5]. In this context, research on light, inexpensive, and more importantly environmentally benign materials becomes a priority to facilitate the technology´s inclusion into the market. One of such materials is the $Mg_2(Si,Sn)$ system, composed of a solid solution of Mg_2Si and Mg_2Sn. Both binaries and their solid solutions form a family of light and highly available (therefore inexpensive) materials [1, 2].

$Mg_2(Si,Sn)$ has shown a good thermoelectric performance, as indicated by the high dimensionless figure of merit zT defined as $zT = S^2\alpha\kappa^{-1}T$, where S, α, κ, and T represent Seebeck coefficient, electrical conductivity, total thermal conductivity, and absolute temperature, respectively. n-type $Mg_2(Si,Sn)$ achieved a $zT > 1.2$ at temperatures close to 973 K [6-12], while p-type materials reached 0.55 around the same temperatures [11, 13-17].

Several other factors besides TE performance have to be taken into account when building a functional generator, such as the electrode that connects the functional material to the electrical bridge. Further progress has been made in this regard with possible candidates already selected and tested. Cu and Ag seem to be feasible options for the Sn-rich solid solutions given their compatible coefficient of thermal expansion (CTE) values [18, 19], while Ni appears to be a solution for binary Mg_2Si [20-22].

The selection of the TE material, the contacting electrode and the bridging electrical conductor is not trivial. In fact, CTE mismatches between these materials will produce thermal stresses at working temperature that could potentially threaten the mechanical integrity of the module. Using the same material system for both n- and p-type legs is one way to reduce the CTE mismatch; it will, however, not completely

eliminate the issue. Therefore, thermal stress and its potentially destructive effects cannot be avoided [23].

It is, thus, imperative to know the room and high temperature mechanical behavior of the materials in order to design the module in a way that minimizes possible mechanical failure.

The mechanical properties of the binary magnesium silicide were predicted using first principles calculations, obtaining a value of 110 GPa for the Young´s modulus [24, 25], and were measured using several techniques. Among these techniques, we find dynamic methods like Resonant Ultrasound Spectroscopy (RUS) and traditional static characterizations like micro-hardness and compression tests [26-29]. These previous studies reported a wide range of values for the elastic behavior of Mg_2Si, ranging from 76 GPa to 145 GPa, with hardness values ranging from 4 to 5.4 GPa. The authors put great emphasis on the effect of grain size distribution on the mechanical properties in these studies.

In contrast, reported data on Mg_2Sn is more limited. First principles calculations for this binary yield a Young´s modulus of 67-82 GPa [25, 30, 31], and an experimental hardness value of 1.7 GPa was reported [12].

Recent work in our research group was done on the mechanical properties of the solid solutions $Mg_2Si_{1-x}Sn_x$ (with x = 0 - 1), finding a mostly linear influence of the Sn content on the hardness. However, $Mg_2Si_{0.6}Sn_{0.4}$ showed an increased value compared to what the interpolation between binaries suggests and above the linear behavior characteristic in the low Si content material. Such behavior was attributed to secondary phases strengthening the material [32]. Room temperature measurements of the elastic constants have also been carried out on the solid solution [33], and the

study found a strengthening of the material as the Si amount increased. However, the composition $Mg_2Si_{0.4}Sn_{0.6}$ showed diminished elastic properties, which was attributed by the authors to a possible connection between electronic and vibrational properties.

On the other hand, high temperature values are scarce. One recent paper reported the Young´s modulus of the $Mg_2Si_{0.6}Sn_{0.4}$ material [34] where a linear decrease with temperature was found. The material had a reduction of ~10% in its total elasticity during the heating phase; however, no further information was given on the cooling phase.

One complication of the Mg_2Si-Mg_2Sn material system is the miscibility gap, which, depending on the author, can be found in different compositional ranges [35, 36]. The gap also depends heavily on temperature, as it widens at lower temperatures. It was observed in previous studies that homogenized samples decompose into separate phases after being annealed. Due to the phase separation at high temperatures, it is of utmost importance to know the material stability while being subjected to temperature.

Therefore, this work focuses on the microstructural and Young´s modulus characterizations of $Mg_2Si_xSn_{1-x}$ materials (x = 0 - 1), at both room and high temperatures using different techniques: Resonant Ultrasound Spectroscopy (RUS) and Impulse Excitation Technique (IET).

2. Materials and methods

Undoped $Mg_2Si_{1-x}Sn_x$ samples were synthesized using commercially available precursor elements, namely Mg turnings (Merck), Si chunks (<6 mm, ChemPur), and Sn (<71 µm, Merck) with high purity >99.5%. Elemental materials were put in a graphite crucible and melted into an ingot using a previously described method [11].

The obtained ingot was then ball milled in a SPEX 8000D Shaker Mill for an hour to obtain a homogenous powder, and pellets were synthesized by pressing the powder in a direct current press DSP 510 SE from Dr. Fritsch GmbH. The temperature and time used to press each composition have been reported previously [6, 11, 19, 36, 37] and are detailed in Table 1. These reports showed very good thermoelectric properties for both n and p-type materials. Samples of compositions $Mg_2Si_{1-x}Sn_x$ x = 0.4, 0.5, 0.6 require extra time for pressing conditions due to the slow process of phase formation. It was previously observed that if Mg_2Sn and Mg_2Si formations are competing, Mg_2Sn forms first and then Si diffuses slowly into the matrix [6, 36].

Table 1. Sintering parameters for $Mg_2Si_{1-x}Sn_x$

x	**Pressure (MPa)**	**Temperature (°C)**	**Time (min)**
0	66	800	10
0.4	66	750	30
0.5	66	700	20
0.6	66	700	20
0.7	66	700	10
1	66	600	10

The pellets obtained measured 50 mm in diameter and ~3 mm in thickness. They were then subsequently cut using a diamond disc saw (DISCO Co) into pieces measuring 12 × 45 × 3.0 mm for the IET experiments and 3.0 x 4.0 x 5.0 mm for the RUS characterization. Two separate samples were cut and tested for each composition and technique. The remaining circular segments were embedded in

conductive resin, grinded with SiC paper and polished with diamond suspension for microstructure analysis.

Resonant ultrasound spectroscopy (RUS) utilizes mechanical resonance frequencies of a given sample to determine the elastic tensor of a material. Parallelepiped shaped polycrystalline samples of 60 mm^3 were investigated by a custom made spectrometer similar to the setup described in [38]. Using the first 20 resonances, C_{11} and C_{44} were determined following the analytical scheme described in [39] and implemented in Python. In all cases, the root-mean-square residual between calculated and measured resonance frequencies was below 0.5%.

Independent elastic constants C_{11}, C_{12} and C_{44} [40] characterized by RUS can then, be related to the elastic moduli. The bulk B modulus can be estimated by the relationship

$$3B = C_{11} + 2C_{12} \qquad \text{Eq. 1}$$

The shear modulus G can be described by Equation 2 for materials with cubic crystal structure.

$$G = C_{44} \qquad \text{Eq. 2}$$

Finally Young´s modulus can be estimated using Equation 3

$$E = \frac{9B \cdot G}{3B + G} \qquad \text{Eq. 3}$$

RUS experiments were carried out in a self-built setup at room temperature sweeping frequencies between 300 kHz and 1 MHz. Characterization was done repeatedly while changing the position of the sample between transducers to maximize the amount of resonant frequencies registered for the fitting.

The Impulse Excitation Technique (IET) relies on the free vibration of a bar shaped sample set on top of supports. A microphone picks up the resulting vibration frequency. A simple set of equations are then used to compute the Young´s and shear modulus.

$$E = 0.9465 \frac{m{F_l}^2}{b} \frac{L^3}{t^3} T_1 \qquad \text{Eq. 4}$$

$$G = \frac{4Lm{F_t}^2}{bt} \frac{B}{1-A} \qquad \text{Eq. 5}$$

Where *m* is the mass of the sample, *L*, *b* and *t* are the length, width and thickness respectively; F_l is the longitudinal resonant frequency and F_t the transverse resonant frequency. T_1, *B* and *A* are all geometrical correction factors described in the standard ASTM E 1876 – 01 [41]. In such a case, it is important to ensure that the fundamental (lowest resonant frequency) has been identified. The ratio to higher order frequencies can be used to determine if the fundamental is present, and whether we measured longitudinal or transverse. For longitudinal frequencies the ratio to the fundamental is 1:2.757:5.404:8.933…; meanwhile, for the transverse, the relationship is simpler, 1:2:3:4…

Slight variations in the thickness of the samples during preparations alter the precision of the method following Eq. 4, therefore we grinded all samples to get a ΔE < 1 GPa.

IET characterization was done employing a system from IMCE NV at room temperature with an automatic excitation time of 30 ms. High temperature measurements were done in air until 673 K, and then the sample was held at this temperature for 30 min. Heating and cooling ramp was 5 K per minute, and one data point was collected every 60 s during both processes. The oven can only control the

cooling ramp down to 423 K; afterwards the cooling through natural convection happens slower.

Phase identification was done using X-ray diffraction, which was performed on sample pellets utilizing a Siemens D5000 Bragg-Brentano diffractometer with a secondary monochromator. Spectra were taken using Cu K_α radiation (1.5406 Å) in the 2θ range 20°-80° with a step size of 0.01°, and the lattice parameters were estimated using the Bragg equation. Microstructure analysis was carried out using a Scanning Electron Microscope Zeiss Ultra 55 SEM with a Zeiss QBSE detector, also equipped with an Oxford energy dispersive X-ray (EDX) detector (PentaFETx3). The grain size was observed from SEM pictures and estimated using ImageJ software.

Density measurements needed for the RUS and IET calculations were obtained using the Archimedes method in ethanol. All samples exhibited relative densities higher than 96%. The solid solution relative density was taken as linear interpolation between the binaries.

3. Results

Most pressed pellets exhibit high phase purity, as shown by the XRD patterns in Figure 1. Samples with x = 0.5 and 0.4 exhibit a shoulder or peak bifurcation. Which could be an indicator that secondary phases are present in the material. Only phases with a composition of $Mg_2Si_{1-x}Sn_x$ were found, i.e. no MgO or elemental Si or Sn (see figure 1. in SI)

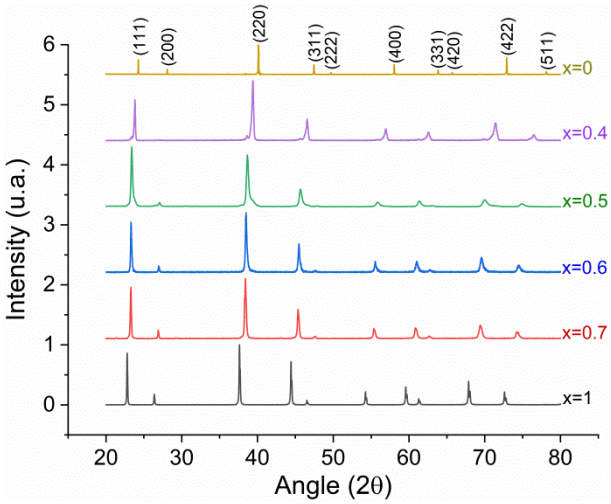

Figure 1. XRD Spectra for the solid solution $Mg_2Si_{1-x}Sn_x$, x = 0-1

Using the main peaks (111) and (220), the Bragg equation was used to estimate the lattice parameter for each sample. The results were then averaged and shown together with density and composition in Table 2 .

Table 2 structural parameters for $Mg_2Si_{1-x}Sn_x$

x	Density (g/cm^3)	Relative density	Lattice parameter (Å)	Grain size (µm)
0	1.97	0.99	6.35	7±1
0.4	2.65	1.00	6.46	8±2
0.5	2.83	1.01	6.58	7±2
0.6	2.97	1.00	6.58	8±2
0.7	3.09	0.99	6.62	7±3
1	3.46	0.96	6.76	7±1

The grain sizes were estimated using image processing software and were found to be very similar for all compositions; this is presumably because of the preparation procedure. While the melting temperature is different between the compositions, the final step before compaction is a one-hour ball milling of the ingot, which is the same for all samples. This similarity between samples means any differences in mechanical properties will not come from grain size difference, but from other sources i.e. Sn-Si ratio, secondary phases amount, etc.

Room temperature IET measurements for $Mg_2Si_{1-x}Sn_x$ (Figure 2. a) show a linear influence of the tin content in the solid solution on the Young´s modulus, with the exception of x = 0.4. This composition does not follow the linear behavior observed for the other compositions.

RUS allows us to characterize the elastic constants (see Table 1. in SI), and then, by using Eq. 1, Eq. 2 and Eq. 3, the moduli were calculated for the samples studied in this work (Figure 2. a). These results also exhibit a linear behavior as the Sn content increases, and go well in accordance with previously reported values [33]. Nevertheless, we observed a reduced elastic constant value at x=0.6, as also previously reported in the same paper.

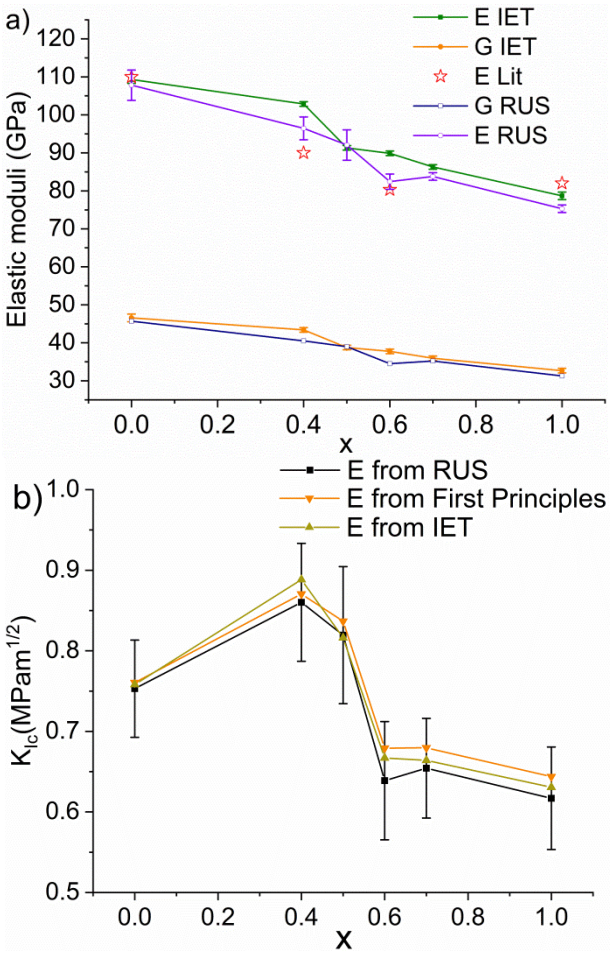

Figure 2. a) Comparison between elastic constants obtained by RUS and IET with literature data [12, 25, 30, 34, 42] and b) Estimation of fracture toughness using (i) values of Young's modulus obtained by linear interpolation between first principles calculation [32] and (ii) experimental observation.

Using previously reported hardness data [32], the fracture toughness of the studied composition along the solid solution was estimated using Equation 6 [32].

$$K_{Ic} = \frac{\zeta (E/H)^{\frac{1}{2}} P}{c^{3/2}} \qquad \text{Eq. 6}$$

where *H* is the measured hardness, *P* the load used for the indentation and *c* the length of the crack as measured from the center of the indentation, ζ is a geometrical correction factor set to be 0.016 [43]. Crack length and diagonal needed for hardness estimation were measured using the in-built microscope as described in [32].

Figure 2. b) shows the difference in K_{Ic} between using first principles and experimental values recorded by RUS and IET measurements for the estimation. $Mg_2Si_{0.6}Sn_{0.4}$ exhibited the highest fracture toughness in the original study with the interpolated Young's modulus. Using the measured value instead does not change the trend.

Previous work predicted a linear decrease in elastic constants above room temperature [25]. This work confirms this behavior, as all the samples show a linear dependence of Young´s modulus with increasing temperature (Figure 3. a).

Mg_2Sn exhibits the highest percentage of softening at high temperature (623 K) with 11%, while the samples containing Si (solid solutions and binary Mg_2Si) only lose 7-

8% of their total strength. Such behavior does not come as a surprise as the stiffening of the $Mg_2(Si,Sn)$ solid solutions were previously described by Klobes *et al.* [33] as the effect of the covalent Mg-Si bond.

Once the material reaches the holding temperature, a small strengthening takes place (<1%), which continues when the cooling process starts, as shown in Figure 3. b). The hysteresis behavior was observed for all samples and is typical of a micro crack healing mechanism that takes place at higher temperatures. Once the material starts to cool down, the thermal stress re-opens micro cracks and the material returns to its original state [44]. It cannot be excluded, however, that the micro-crack healing process starts before the holding temperature. However, with the employed measurement approach, it is noticeable only when the maximum testing temperature is reached, and the temperature-induced decrease in Young´s modulus ceases.

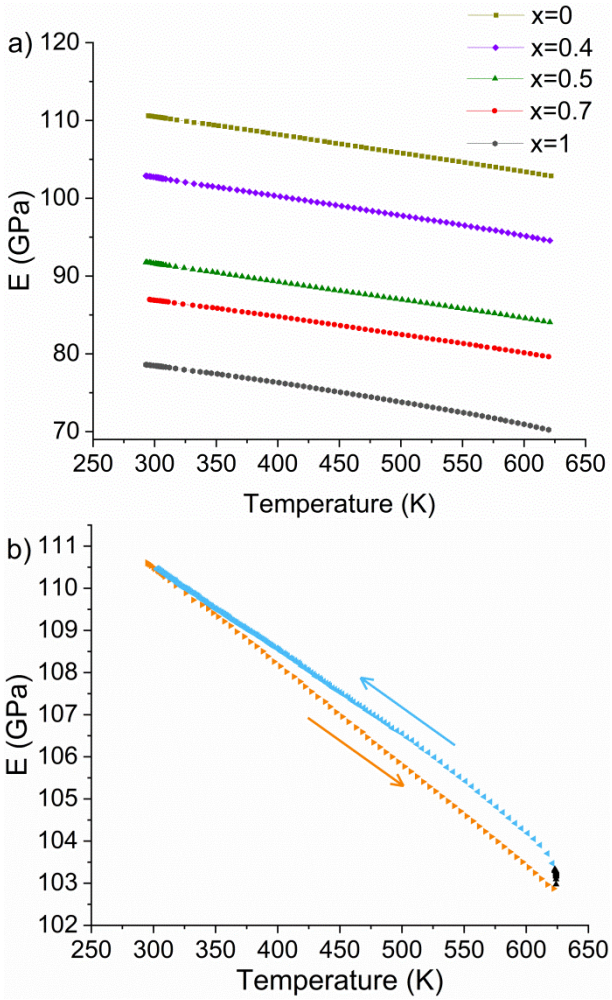

Figure 3. a) Heating curve for high temperature measurements of Young´s modulus showing all compositions tested and b) heating and cooling curve for Mg_2Si, showing a noticeable hysteresis.

The integrity of the microstructure after the measurement cycle can be attested by the fact that the initial value is reached again at room temperature. Furthermore, previous work in the research group has proven that long time annealing of samples obtained through the very same method retains the microstructure [11].

The setup used to test high temperature Young´s modulus does not permit the easy characterization of shear modulus. However, it can be derived using the Poisson ratio, which is defined as $\nu = \frac{E}{2G} - 1$.

In this regard, we find one previous report of Poisson's ratio measurement for the solid solution x = 0.6 [12] which shows a small increase from 0.197 to 0.215 in the temperature range from 300 K to 600 K. Meanwhile, a calculation made with data obtained from first principles calculations [25] yields values for the binary materials that range from 0.173 to 0.176 for Mg_2Si and 0.20-0.198 for Mg_2Sn in the same temperature range. Therefore, assuming a constant Poisson ratio which was obtained from the room temperature measurements, we calculated the temperature-dependent shear modulus for the complete range of compositions tested in this work, as seen in Figure 4.

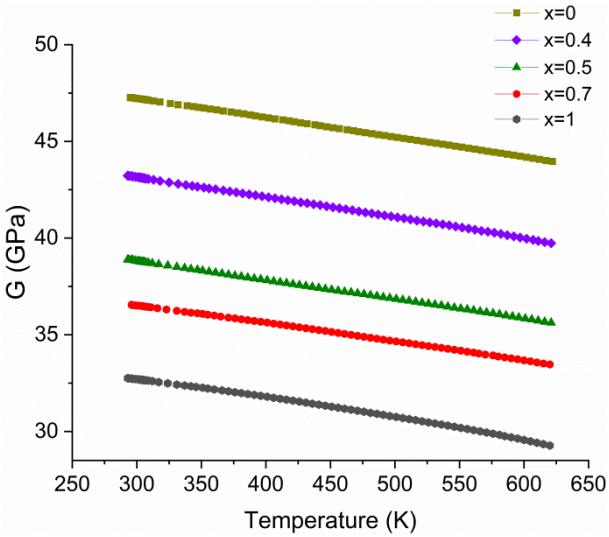

Figure 4. Temperature dependent shear modulus obtained from E(T) and the Poisson ratio at room temperature

The phase purity can be assessed from the microstructure shown in Figure 5. Secondary phases are present to some degree in all solid solution samples. However, only the samples with x = 0.4 and 0.5 have secondary phases in such size and concentration as to be observable in XRD patterns; this is confirmed by the displayed SEM pictures.

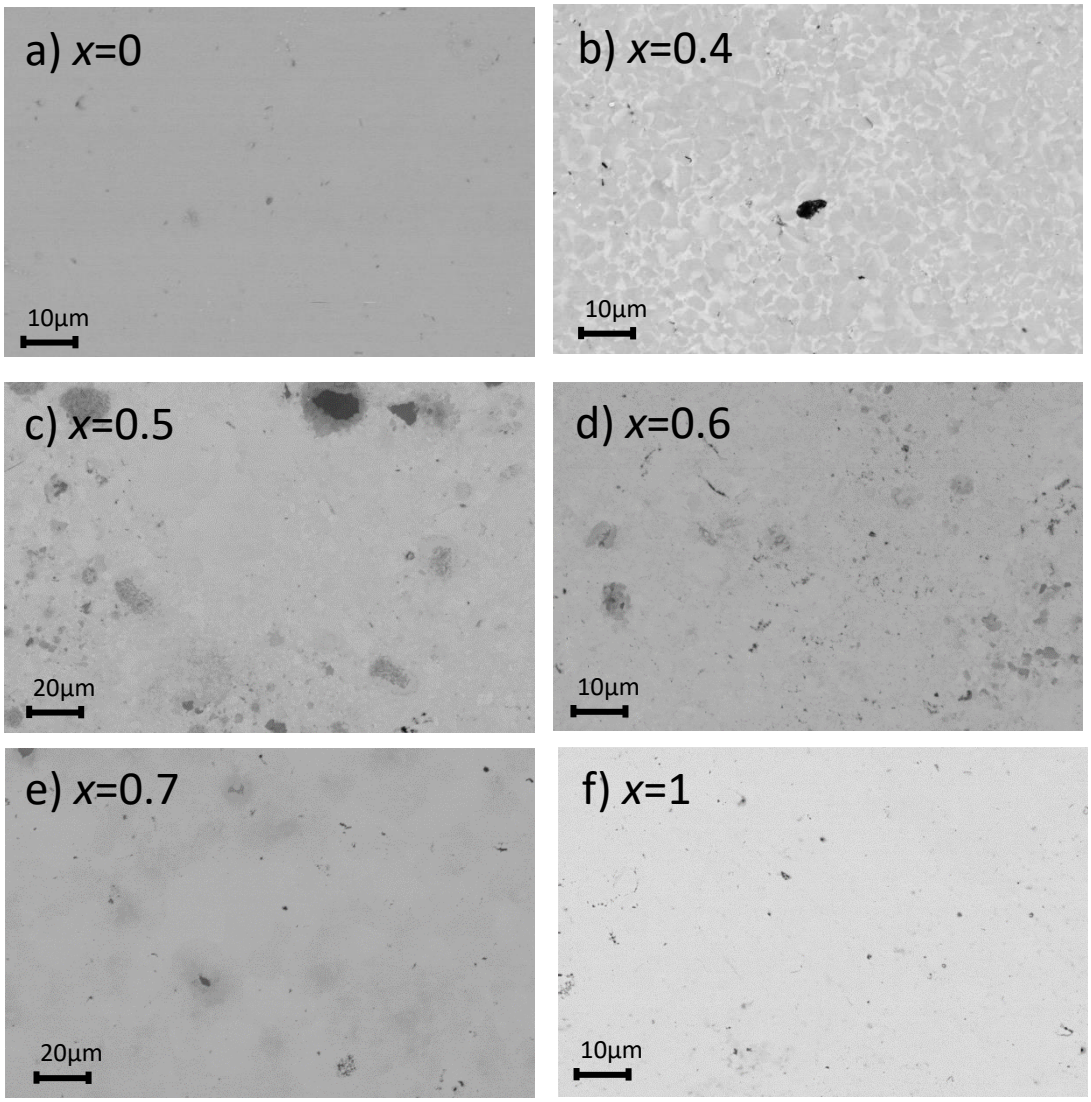

Figure 5. Backscatter SEM images of a) Mg_2Si, b) $Mg_2Si_{0.6}Sn_{0.4}$, c) $Mg_2Si_{0.5}Sn_{0.5}$, d) $Mg_2Si_{0.4}Sn_{0.6}$, e) $Mg_2Si_{0.3}Sn_{0.7}$ and f) Mg_2Sn, dark areas show the secondary Si rich phases in the solid solution.

Figure 5. c), d) and e) show the typical microstructure for the solid solution Mg_2Si-Mg_2Sn with secondary phases rich in Si, typical for a melting route synthesis. The appearance of such secondary phases is due to the incomplete diffusion, which is a consequence of a short pressing time during sintering [6, 36]. Longer sinter times produce purer samples with fewer amounts of Si-rich phases. However, excessive time can also induce Mg loss, which is detrimental to phase formations [36].

Phase quantification in backscatter SEM pictures was done following the methodology described in [45] for two samples, $Mg_2Si_{0.6}Sn_{0.4}$ and $Mg_2Si_{0.3}Sn_{0.7}$, and the results are presented in Figure 6.

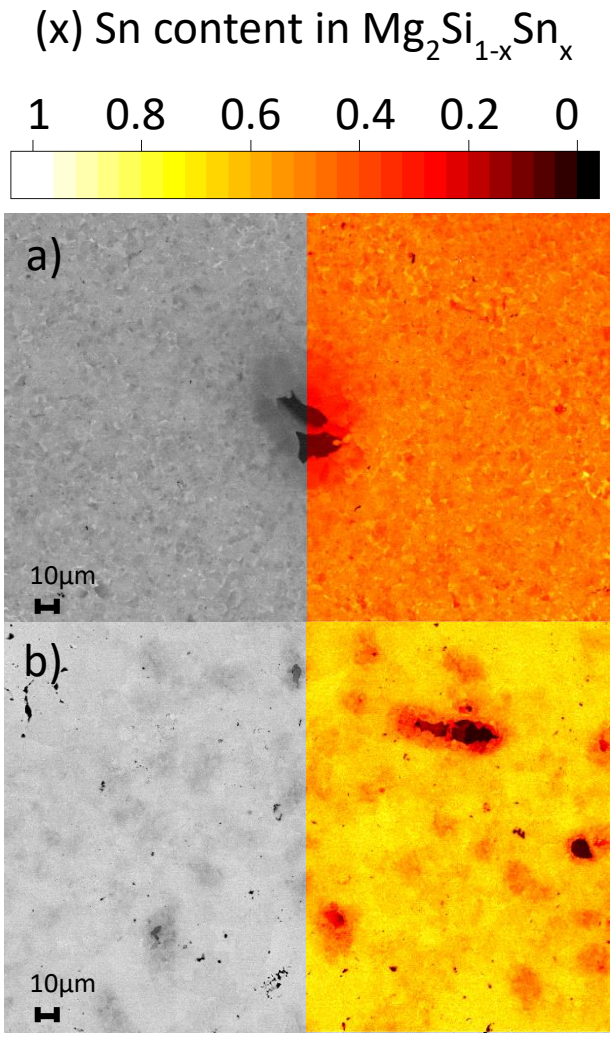

Figure 6. Backscatter SEM pictures and their respective phase quantification for the samples a) $Mg_2Si_{0.6}Sn_{0.4}$ and b) $Mg_2Si_{0.3}Sn_{0.7}$.

The sample x = 0.4 is shown in Figure 6. a). It shows a bifurcated peak in XRD, and phase quantification confirms the incomplete phase homogenization. Sn-rich phases can be seen surrounding phases with greater Si content creating many interfaces, which will introduce further strain into the matrix according to the inclusion theory

[46]. These additional strains might be the reason for the observed increase in Young's modulus. On the other hand, the sample with *x* = 0.7 shown in Figure 6. b) has a better phase purity, confirming the XRD measurements. The matrix (orange) is noticeable in the picture, and embedded within it, we can identify particles with higher Si content (shown as darker shade of red) and reddish diffusion zones around them. The cumulative percentage of phases belonging to specific compositions (see figure 5. In SI) shows that the target phase with Δx=0.2 composes more than 90% of the area. These diffusion zones confirm the observations done by Yasseri *et al.* [36] that Si-rich $Mg_2(Si,Sn)$ remnant from the synthesis reacts in the sintering phase as the Si slowly substitutes Sn in the matrix, dissolving the Mg_2Si. Additionally, binary Mg_2Si can also be identified in both pictures.

Given the comparatively low variation in Young's modulus values for $Mg_2Si_{1-x}Sn_x$ and, assuming the area depicted in the SEM picture is representative of the volume fraction of secondary phases in the rest of the material, we can expect very little change in the effective Young's modulus measured. This is because to estimate the elastic modulus in composite materials the contributions of each phase are considered linearly in the Voigt approximation ($\bar{E} = \sum_i n_i E_i$) and approximately linearly in the Reuss approximation ($\bar{E} = \sum_i n_i / {E_i}^{-1}$) [47].

Previous studies on $Mg_2(Si,Sn)$ obtained through the same method described in this work have shown no indication of microstructural change after annealing at 723K for more than 700 Hours [11]. It is therefore assumed that the thermal cycle experienced by the samples during the measurement did not affect the microstructure present in the pristine samples.

4. Discussion

Previous reports for the Young´s modulus of Mg_2Si show similar values to what we report,109 GPa [26-29], except for a value of 145 GPa obtained through nano-indentation [28]. With regard to that characterization technique, Radison *et al.* [48] proved that nano-indentation is a good method to characterize the Young´s modulus of a material, yet it was also prone to overestimate the value. This might be the reason for the considerable discrepancy between what we present in this work for the binary material and previous reports by Muthiah *et al* [28].

RUS and IET were compared in the past by Radovic *et al.* [48]. The paper describes thickness as the main source of uncertainty in IET. As much as 9% variation in elastic moduli can be expected with a variation of thickness below 3%. In our study, the maximum variation for the samples following the linear behavior was 5%, which is well within the previously reported precision for the techniques used. The outliers from linearity are probably due to different effects, such as the inhomogeneity for the x = 0.4 composition and the possible influence of the band convergence on the vibrational properties for the x = 0.6 sample, rather than technique-dependent uncertainties.

Fracture toughness values do not deviate widely from each other due to the fact that the Young´s modulus measurements agree with the linear interpolation used in the first study [32]. Said work also described the effect of secondary phases and particle sizes as strengthening factors in the material. Such mechanisms can be observed in samples with $x < 0.5$. In this case, the high concentration of interfaces is likely to deflect or shorten cracks due to the intergranular energy at the particle boundaries [49].

The temperature dependent elastic behavior in polycrystalline materials, in general, can be divided into three regions, of which the first two can be described by the empirical Wachtman equation $E = E_0 - bTe^{-\frac{T_0}{T}}$ where E_0 is the Young´s modulus at 0 K, b and T_0 are constants [50]. Previous work has set T_0 to 0.3-0.5 Debye temperature (θ_D) [51].

Beginning at the low temperature of ~0.3 θ_D, the slope *dE/dT* decreases as $e^{-\frac{T_0}{T}}$ increases gradually with temperatures falling down to 0 K, where $E = E_0$. Above 0.3 θ_D we find the linear region where *dE/dT* remains constant as $e^{-\frac{T_0}{T}}$ approaches unity. Finally, the high temperature regime can no longer be described by the Wachtman equation, because the slope deviates from linearity as it gradually increases. The onset of such slope change depends on the material and can be obtained experimentally [51]. Thus, in order to identify the region where this experiment takes place, we estimated the Debye temperature.

For that, the average acoustic sound velocity was calculated using Equation 7

$$v_{\mathrm{m}} = \left(\frac{1}{3}\left[\frac{2}{{v_s}^3} + \frac{1}{{v_l}^3}\right]\right)^{-1/3} \qquad \text{Eq. 7}$$

Where v_s is the transverse acoustic velocity ($v_s = \sqrt{\frac{G}{\rho}}$) and v_l is the longitudinal acoustic velocity ($v_l = \sqrt{\frac{E}{\rho}}$) [52]. Then the acoustic Debye temperature was estimated as

$$\theta_{\mathrm{D}} = \frac{h}{k_{\mathrm{B}}}\left(\frac{3q}{4\pi}\frac{N_A\rho}{M}\right)^{1/3} v_{\mathrm{m}}\ , \qquad \text{Eq. 8}$$

where h and k_{B} are the Plank and Boltzmann constants, q is the number of atoms per molecule, M the molecular weight, N_A the Avogadro number and ρ the material

density. Results for v_l, v_s, v_{m} and θ_{D} are shown in Table 3 . The presented data has an uncertainty of 20 m/s for sound velocities and 5 K for the Debye temperature.

Table 3 Room temperature sound velocities: longitudinal (v_l) shear (v_s) and average (v_m); as well as Debye temperature (θ_D) for the solid solution $Mg_2Si_{1-x}Sn_x$

x	V_l (m/s)	V_s (m/s)	V_m (m/s)	θ_D (K)
0	7730	4860	5350	570
0.4	6510	4040	4460	460
0.5	5920	3700	4080	420
0.6	5760	3560	3930	400
0.7	5560	3410	3760	380
1	5040	3080	3400	340

With the Debye temperature and the Wachtmann model, we can expect the high temperature values for Young´s modulus to be linear, as 0.3-0.5 θ_D is well below the temperature range of this study for all compositions.

The high temperature behavior of elastic moduli was predicted [25] and experimentally observed to be a linear decrease for $Mg_2Si_{0.4}Sn_{0.6}$ [12] and $Mg_2Si_{0.6}Sn_{0.4}$ [34], which is in agreement with our results. Both previous studies report a reduction of 5-10% in the characterized elastic constants. In the previous work [34], the behavior of the $Mg_2Si_{0.4}Sn_{0.6}$ sample was fitted using a linear function and had a very good coefficient of determination (R^2 = 0.995) in the temperature range 300-600 K.

Our results, as well as previous literature reports, therefore indicate the validity of using a bilinear function in the form $A(x,T) = A_r + bT + cx$.

For this linear equation, A_r is either modulus at 0 K, Young´s modulus (*E*) or shear modulus (*G*). The values used to fit the equation are detailed in Table 4 including the coefficient of determination obtained as described in [53]. Here the sample with $x = 0.4$ was excluded from the fitting due to the observed poor phase quality. However, as can be seen for the results including $x = 0.4$ (see SI), the coefficient of determination was very lightly modified.

Table 4. Values used to fit the model from room temperature up to 600K

Modulus	**A_r (GPa)**	**b (GPa K^{-1})**	**c (GPa)**	**R^2**
Young´s modulus	116.55	-0.0234	-32.032	0.99
Shear modulus	49.77	-0.0098	-14.513	0.99

Table 4. allows for the thermomechanical modelling of a TEG under operational conditions, and for an optimization with respect to composition, taking mechanical properties into account. The prediction of lattice thermal conductivities can also benefit from more precise data of the mechanical properties. A previous work on $Mg_2Si_{1-x}Sn_x$ materials [54] estimated the lattice thermal conductivity using the Debye approximation in the form $\kappa_l = \frac{k_B}{2\pi V_m}\left(\frac{k_B T\pi}{h}\right)\frac{x^4 e^x}{(e^x-1)^2}\tau_c$ where we see the average sound velocity v_m. The approximation also depends on the Boltzmann constant k_B, the Plank constant h and the reduced phonon energy *y* which in turn is estimated with $y = \frac{2h\omega}{k_B T\pi}$ where *ω* is the phonon frequency.

Knowledge of the elastic constants is also important for the modelling of the electronic properties. Scattering by acoustic phonons is the dominant scattering mechanism for electrons above room temperature for most materials [9, 55]. This interaction is characterized by the deformation potential E_{Def} which is related to the carrier mobility by $\mu \propto \frac{C_l}{E_{\mathrm{Def}}^2 \cdot m^{*2.5}}$, where m^* is the carrier effective mass and C_l is given by $C_l = E - G$ for cubic crystals [40]. Practically, E_{Def} is usually obtained from the measured mobility at high temperature using room temperature values for E and G [37, 55-58]. However, as both exhibit clear temperature dependence, this leads to incorrect values of E_{Def} and should be considered as a fair approximation only.

5. Conclusion

High temperature elastic constants, as well as hardness and fracture toughness, are important parameters to predict the mechanical behavior of a certain material under load. Knowledge of said parameters will allow to thermo-mechanically model a possible TEG manufactured using $Mg_2Si_{1-x}Sn_x$, with correct values for the mechanical properties under application conditions.

Elastic moduli *E* and *G* are presented for several compositions along the $Mg_2Si_{1-x}Sn_x$ ($x = 0 - 1$) solid solution series at both room and high temperatures. The first ever experimental value for binary polycrystalline Mg_2Sn is presented and is in good agreement with first principles calculations. It was also shown that both the temperature and composition have a linear influence on both the moduli, which facilitates the description of the behavior by a simple bilinear equation.

Additionally, we describe that, besides a prominence of secondary phases, phase distribution can also affect the elastic behavior by stiffening the material, as was the case with the Si-rich (x = 0.4) $Mg_2Si_{1-x}Sn_x$. $Mg_2Si_{0.6}Sn_{0.4}$ was the only sample to deviate from the linear decrease in Young´s modulus in the IET measurements. Such behavior is closely related to the microstructure found in the material, where small Si-rich areas are found surrounded by Sn-rich phases, creating a biphasic material with a great amount of interfaces.

$Mg_2Si_{0.4}Sn_{0.6}$, on the other hand, deviated from the linear behavior in the RUS characterization. This is well in agreement with previous reports and possibly a consequence of the convergence of the conduction bands in this composition.

A better estimation of the temperature dependent elastic moduli is not only beneficial for mechanical design and modelling, but also for electronic and thermal properties of the thermoelectric materials.

6. Acknowledgements

The authors would like the acknowledge the endorsement for the DLR executive Board Members for Space Research and Technology, as well as the financial support from the Young Research Group Leader Program.

Financial support for M.Y is provided by the DFG via the GRK (Research Training Group) 2204 "Substitute Materials for Sustainable Energy Technologies“. GCH would like to thank the Mexican science and technology council (CONACyT) and the German academic exchange service (DAAD) for the PhD fellowship.

7. References

[1] X.D. Luo, H. Liu, W.L. Xu, Y.X. Zhu, Progress on Mg2Si thermoelectric materials, Adv Mater Res-Switz 886 (2014) 71-74.

[2] R. Santos, S.A. Yamini, S.X. Dou, Recent progress in magnesium-based thermoelectric materials, J Mater Chem A 6(8) (2018) 3328-3341.

[3] D.M. Rowe, Thermoelectric-Power Generation, Iee Rev 125(Nov) (1978) 1113-1136.

[4] D.M. Rowe, Applications of Nuclear-Powered Thermoelectric Generators in Space, Appl Energ 40(4) (1991) 241-271.

[5] S. LeBlanc, S.K. Yee, M.L. Scullin, C. Dames, K.E. Goodson, Material and manufacturing cost considerations for thermoelectrics, Renew Sust Energ Rev 32 (2014) 313-327.

[6] A. Sankhla, A. Patil, H. Kamila, M. Yasseri, N. Farahi, E. Mueller, J. de Boor, Mechanical Alloying of Optimized Mg2(Si,Sn) Solid Solutions: Understanding Phase Evolution and Tuning Synthesis Parameters for Thermoelectric Applications, ACS Applied Energy Materials 1(2) (2018) 531-542.

[7] V.K. Zaitsev, M.I. Fedorov, E.A. Gurieva, I.S. Eremin, P.P. Konstantinov, A.Y. Samunin, M.V. Vedernikov, Highly effective Mg2Si1-xSnx thermoelectrics, Phys. Rev. B 74(4) (2006) 045207.

[8] W. Liu, X.J. Tan, K. Yin, H.J. Liu, X.F. Tang, J. Shi, Q.J. Zhang, C. Uher, Convergence of Conduction Bands as a Means of Enhancing Thermoelectric Performance of n-Type Mg2Si1-xSnx Solid Solutions, Phys. Rev. Lett. 108(16) (2012) 166601.

[9] W. Liu, H. Chi, H. Sun, Q. Zhang, K. Yin, X. Tang, Q. Zhang, C. Uher, Advanced thermoelectrics governed by a single parabolic band: Mg2Si(0.3)Sn(0.7), a canonical example, Phys Chem Chem Phys 16(15) (2014) 6893-7.

[10] T. Dasgupta, C. Stiewe, J. de Boor, E. Müller, Influence of power factor enhancement on the thermoelectric figure of merit in Mg2Si0.4Sn0.6based materials, physica status solidi (a) 211(6) (2014) 1250-1254.

[11] N. Farahi, C. Stiewe, D.Y.N. Truong, J. de Boor, E. Muller, High efficiency Mg-2(Si,Sn)-based thermoelectric materials: scale-up synthesis, functional homogeneity, and thermal stability, Rsc Adv 9(40) (2019) 23021-23028.

[12] P. Gao, I. Berkun, R.D. Schmidt, M.F. Luzenski, X. Lu, P.B. Sarac, E.D. Case, T.P. Hogan, Transport and Mechanical Properties of High-ZT Mg2.08Si0.4-x Sn0.6Sb (x) Thermoelectric Materials, J Electron Mater 43(6) (2014) 1790-1803.

[13] H. Kamila, A. Sankhla, M. Yasseri, P. Hoang, N. Farahi, E. Mueller, J. de Boor, Synthesis of p-type Mg2Si1-xSnx with x = 0-1 and optimization of the synthesis parameters, Materials Today: Proceedings 8 (2019) 9.

[14] J. de Boor, T. Dasgupta, U. Saparamadu, E. Müller, Z.F. Ren, Recent progress in p-type thermoelectric magnesium silicide based solid solutions, Materials Today Energy 4 (2017) 105-121.

[15] P. Gao, J.D. Davis, V.V. Poltavets, T.P. Hogan, The p-type Mg2LixSi0.4Sn0.6 thermoelectric materials synthesized by a B2O3 encapsulation method using Li2CO3 as the doping agent, J Mater Chem C 4(5) (2016) 929-934.

[16] P. Nieroda, A. Kolezynski, M. Oszajca, J. Milczarek, K.T. Wojciechowski, Structural and Thermoelectric Properties of Polycrystalline p-Type Mg2-x Li (x) Si, J Electron Mater 45(7) (2016) 3418-3426.

[17] U. Saparamadu, J. de Boor, J. Mao, S.W. Song, F. Tian, W.S. Liu, Q.Y. Zhang, Z.F. Ren, Comparative studies on thermoelectric properties of p-type Mg2Sn0.75Ge0.25 doped with lithium, sodium, and gallium, Acta Mater 141 (2017) 154-162.

[18] S. Ayachi, G. Castillo-Hernandez, M. Yasseri, J. de Boor, E. Müller, Developing Contacting Solutions for Mg2Si1–xSnx-Based Thermoelectric Generators: Cu and Ni45Cu55 as Potential Contacting Electrodes, Acs Appl Mater Inter (2019).
[19] N.P. Pham, N. Farahi, H. Kamila, A. Sankhla, S. Ayachi, E. Müller, J. de Boor, Ni and Ag electrodes for magnesium silicide based thermoelectric generators, Materials Today Energy 11 (2019).
[20] J. De Boor, D. Droste, C. Schneider, J. Janek, E. Mueller, Thermal Stability of Magnesium Silicide/Nickel Contacts, J Electron Mater 45(10) (2016) 5313-5320.
[21] J. de Boor, C. Gloanec, H. Kolb, R. Sottong, P. Ziolkowski, E. Muller, Fabrication and characterization of nickel contacts for magnesium silicide based thermoelectric generators, J Alloy Compd 632 (2015) 348-353.
[22] K. Mitra, S. Mahapatra, T.J.J.o.E.M. Dasgupta, Fabrication of Nickel Contacts for Mg2Si Based Thermoelectric Generators via an Induction Assisted Rapid Monoblock Sintering Technique, 48(3) (2019) 1754-1757.
[23] X.D. Jia, Y.W. Gao, Estimation of thermoelectric and mechanical performances of segmented thermoelectric generators under optimal operating conditions, Appl Therm Eng 73(1) (2014) 335-342.
[24] Z.W. Huang, Y.H. Zhao, H. Hou, P.D. Han, Electronic structural, elastic properties and thermodynamics of Mg17Al12, Mg2Si and Al2Y phases from first-principles calculations, Physica B 407(7) (2012) 1075-1081.
[25] S. Ganeshan, S.L. Shang, Y. Wang, Z.K. Liu, Temperature dependent elastic coefficients of Mg2X (X = Si, Ge, Sn, Pb) compounds from first-principles calculations, J Alloy Compd 498(2) (2010) 191-198.
[26] R.D. Schmidt, E.D. Case, J. Giles, J.E. Ni, T.P. Hogan, Room-Temperature Mechanical Properties and Slow Crack Growth Behavior of Mg2Si Thermoelectric Materials, J Electron Mater 41(6) (2012) 1210-1216.
[27] R.D. Schmidt, X.F. Fan, E.D. Case, P.B. Sarac, Mechanical properties of Mg2Si thermoelectric materials with the addition of 0-4 vol% silicon carbide nanoparticles (SiCNP), J Mater Sci 50(11) (2015) 4034-4046.
[28] S. Muthiah, R.C. Singh, B.D. Pathak, A. Dhar, Mechanical properties of thermoelectric n-type magnesium silicide synthesized employing in situ spark plasma reaction sintering, Mater Res Express 4(7) (2017).
[29] V. Milekhine, M.I. Onsoien, J.K. Solberg, T. Skaland, Mechanical properties of FeSi (epsilon), FeSi2 (zeta(alpha)) and Mg2Si, Intermetallics 10(8) (2002) 743-750.
[30] W.B.W. L.C.Davis, G.C.Danielson, Elastic constants and calculated lattice vibration frequencies of Mg2Sn, J Phys Chem Solids 28(3) (1967) 9.
[31] X. Li, H. Xie, B. Yang, S.M. Li, Elastic and Thermodynamic Properties Prediction of Mg2Sn and MgTe by First-Principle Calculation and Quasi-Harmonic Debye Model, J Electron Mater (2019).
[32] G. Castillo-Hernandez, M. Yasseri, S. Ayachi, J. de Boor, E. Müller, Hardness and fracture toughness of solid solutions of Mg2Si and Mg2Sn, Fizika i Technika Poluprovodnikov (Semiconductors) (2019).
[33] B. Klobes, J. de Boor, A. Alatas, M.Y. Hu, R.E. Simon, R.P. Hermann, Lattice dynamics and elasticity in thermoelectric Mg2Si1-xSnx, Phys Rev Mater 3(2) (2019).
[34] M. Mejri, Y. Thimont, B. Malard, C. Estournes, Characterization of the thermo-mechanical properties of p-type (MnSi1.77) and n-type (Mg2Si0.6Sn0.4) thermoelectric materials, Scripta Mater 172 (2019) 28-32.
[35] R. Viennois, P. Jund, C. Colinet, J.C. Tedenac, Defect and phase stability of solid solutions of Mg2X with an antifluorite structure: An ab initio study, J Solid State Chem 193 (2012) 133-136.

[36] M. Yasseri, A. Sankhla, H. Kamila, R. Orenstein, D.Y.N. Truong, N. Farahi, J. de Boor, E. Mueller, Solid solution formation in Mg2(Si,Sn) and shape of the miscibility gap, Acta Mater (2019).
[37] H. Kamila, A. Sankhla, M. Yasseri, N.P. Hoang, N. Farahi, E. Mueller, J. de Boor, Synthesis of p-type Mg2Si1-xSnx with x = 0-1 and optimization of the synthesis parameters, Materials Today: Proceedings 8 (2019) 546-555.
[38] D. Bessas, E. Bruck, A versatile Lock-In digital Amplifier (LIdA): the case of mechanical resonances, Eur J Phys 38(3) (2017).
[39] A. Migliori, J.L. Sarrao, W.M. Visscher, T.M. Bell, M. Lei, Z. Fisk, R.G. Leisure, Resonant Ultrasound Spectroscopic Techniques for Measurement of the Elastic-Moduli of Solids, Physica B 183(1-2) (1993) 1-24.
[40] M. Jamal, S.J. Asadabadi, I. Ahmad, H.A.R. Aliabad, Elastic constants of cubic crystals, Comp Mater Sci 95 (2014) 592-599.
[41] ASTM, Dynamic Young's Modulus, Shear Modulus, and Poisson's Ratio by Impulse Excitation of Vibration, 2001.
[42] W.B. Whitten, P.L. Chung, G.C. Danielson, Elastic constants and lattice vibration frequencies of Mg2Si, J Phys Chem Solids 26 (1965).
[43] W.C. Oliver, G.M. Pharr, An Improved Technique for Determining Hardness and Elastic-Modulus Using Load and Displacement Sensing Indentation Experiments, J Mater Res 7(6) (1992) 1564-1583.
[44] J.E. Ni, E.D. Case, R.D. Schmidt, C.I. Wu, T.P. Hogan, R.M. Trejo, E. Lara-Curzio, M.G. Kanatzidis, Fracture mode, microstructure and temperature-dependent elastic moduli for thermoelectric composites of PbTe-PbS with SiC nanoparticle additions, Philos Mag 93(35) (2013) 4412-4439.
[45] M. Yasseri, N. Farahi, K. Kelm, E. Mueller, J. de Boor, Rapid determination of local composition in quasi-binary, inhomogeneous material systems from backscattered electron image contrast, Materialia 2 (2018).
[46] T. Mura, Micromechanics of defects in solids, 2nd, rev. ed., M. Nijhoff

[47] B. Liu, X. Feng, S.M. Zhang, The effective Young's modulus of composites beyond the Voigt estimation due to the Poisson effect, Compos Sci Technol 69(13) (2009) 2198-2204.
[48] M. Radovic, E. Lara-Curzio, L. Riester, Comparison of different experimental techniques for determination of elastic properties of solids, Mat Sci Eng a-Struct 368(1-2) (2004) 56-70.
[49] M.E. Launey, R.O. Ritchie, On the Fracture Toughness of Advanced Materials, Adv Mater 21(20) (2009) 2103-2110.
[50] M.L. Nandanpawar, S. Rajagopalan, Wachtman Equation and Temperature-Dependence of Bulk Moduli in Solids, J Appl Phys 49(7) (1978) 3976-3979.
[51] R.D. Schmidt, E.D. Case, J.E. Ni, J.S. Sakamoto, R.M. Trejo, E. Lara-Curzio, Temperature-dependent Young's modulus, shear modulus and Poisson's ratio of p-type Ce0.9Fe3.5Co0.5Sb12 and n-type Co0.95Pd0.05Te0.05Sb3 skutterudite thermoelectric materials, Philos Mag 92(6) (2012) 727-759.
[52] L. Zhang, G. Rogl, A. Grytsiv, S. Puchegger, J. Koppensteiner, F. Spieckermann, H. Kabelka, M. Reinecker, P. Rogl, W. Schranz, M. Zehetbauer, M.A. Carpenter, Mechanical properties of filled antimonide skutterudites, Mater Sci Eng B-Adv 170(1-3) (2010) 26-31.
[53] C.R. Rao, Linear Statistical Inference and its Applications, John Wiley & Sons, Inc.1973.

[54] G.Y. Jiang, J. He, T.J. Zhu, C.G. Fu, X.H. Liu, L.P. Hu, X.B. Zhao, High Performance Mg2(Si,Sn) Solid Solutions: a Point Defect Chemistry Approach to Enhancing Thermoelectric Properties, Adv Funct Mater 24(24) (2014) 3776-3781.
[55] J. de Boor, T. Dasgupta, H. Kolb, C. Compere, K. Kelm, E. Mueller, Microstructural effects on thermoelectric efficiency: A case study on magnesium silicide, Acta Mater. 77(0) (2014) 68-75.
[56] H. Kamila, P. Sahu, A. Sankhla, M. Yasseri, H.-N. Pham, T. Dasgupta, E. Mueller, J. de Boor, Analyzing transport properties of p-type Mg2Si–Mg2Sn solid solutions: optimization of thermoelectric performance and insight into the electronic band structure, Journal of Materials Chemistry A 7(3) (2019) 1045-1054.
[57] A.F. May, E. Flage-Larsen, G.J. Snyder, Electron and phonon scattering in the high-temperature thermoelectric La3Te4-zMz (M=Sb,Bi), Phys. Rev. B 81(12) (2010).
[58] X.H. Liu, T.J. Zhu, H. Wang, L.P. Hu, H.H. Xie, G.Y. Jiang, G.J. Snyder, X.B. Zhao, Low Electron Scattering Potentials in High Performance Mg2Si0.45Sn0.55 Based Thermoelectric Solid Solutions with Band Convergence, Adv. Energy Mater. 3(9) (2013) 1238-1244.